Acta Geologica Polonica, Vol. 73 (2023), No. 4, pp. 833–851
DOI: 10.2445/agp.2023.148025

Rutile to tourmaline index – a tool for the recognition of the hydrodynamics of the depositional environment; a case study from the Campanian Szozdy Delta System, SE Poland

MICHAŁ CYGLICKI[1, 2] and ZBIGNIEW REMIN[1]

[1] *University of Warsaw, Faculty of Geology, Żwirki i Wigury 93, 02-089 Warszawa, Poland; e-mails: mcyglicki@uw.edu.pl; zremin@uw.edu.pl*
[2] *Polish Geological Institute-National Research Institute, Rakowiecka 4, 00-975 Warszawa, Poland.*

ABSTRACT:

Cyglicki, M. and Remin, Z. 2023. Rutile to tourmaline index – a tool for the recognition of the hydrodynamics of the depositional environment; a case study form the Campanian Szozdy Delta System, SE Poland. *Acta Geologica Polonica*, **73** (4), 833–851. Warszawa.

The newly discovered mid-Campanian Szozdy Delta System (Roztocze Hills, SE Poland) located in the southern part of the Polish Cretaceous Basin, at the northern edge of the Łysogóry-Dobrogea Land, has revealed interesting features concerning the relationship between the abundance of rutile and tourmaline. A distinct inverse relationship between rutile and tourmaline can be readily recognised in the succeeding units of the tripartite cyclothems (calcareous mudstone, calcareous sandstone, and calcareous gaize) representing the submarine part of the Szozdy Delta System. In the Szozdy section, both minerals are of similar shape (highly rounded), durability, and size; they are, however, characterised by markedly different densities. Therefore, it might be expected that these two mineral phases will be strongly dependent, both vertically and spatially, on the local energy of the sedimentary environment hydrodynamic power that existed during the deposition of the succeeding units of the cyclothems. The lighter tourmaline was likely transported further to the more quiescent prodelta environment, rendering the prodelta facies overrepresented in this mineral, whereas the heavier rutile was deposited closer to the river discharge. Such relative change in the abundance of these two mineral phases, emphasised by a standardised Z-score statistics, is referred here to as rutile to tourmaline index (RuTidx). Accordingly, as the RuTidx increases, the hydrodynamic power in the sedimentary environment increases as well. Since these two mineral phases are comparatively immune to alteration during the sedimentary cycle, the RuTidx is considered here to be an independent tool in recognising the hydrodynamics of the depositional environments of any age.

Key words: Sedimentology; Rutile to tourmaline index (RuTidx); Heavy minerals; Hydrodynamics; Sedimentary environment; Hydraulic sorting.

INTRODUCTION

Heavy mineral analysis is amongst the most sensitive and commonly used techniques in the determination of provenance in sandstone and siliciclastic-rich deposits, revealing the depositional and pre-depositional sediment history (e.g., Morton and Hallsworth 1994, 1999, 2007; Frihy 2007; Nauton-Fourteu *et al.* 2021). The composition of heavy mineral assemblages is influenced by three key processes: physical sorting, mechanical abrasion, and dissolution. Physical sorting occurs due to the hydrodynamic

conditions prevailing during the transportation and deposition phases, exerting control over both the absolute and relative concentrations of heavy minerals. Mechanical abrasion occurs in the course of transportation, leading to grain size reduction through a combination of fracturing and rounding. Dissolution, on the other hand, results in the partial or complete loss of heavy minerals under various geochemical conditions at different stages of the sedimentation cycle. These stages include weathering at the source, subaerial exposure in non-marine depositional settings, burial, and, finally, weathering at the outcrop (e.g., Morton and Hallsworth 1994, 1999, 2007; Frihy 2007; Garzanti and Andò 2007; Nauton-Fourteu *et al.* 2021).

Hydraulic sorting can completely transform the heavy mineral complexity by affecting the percentage of individual minerals (Garzanti and Andò 2007). Hydraulic sorting is directly related to flow velocities, especially in the bottom portion of the water column, where most transport processes occur. The flow velocities can be directly translated into threshold stress, which is responsible for selective entrainment and transport. Another important issue is settling velocities, which depend on a number of factors, the most important being the density and diameter of the particle, as well as the shape of the grain. Also important is the kinematic viscosity of the medium in which the grain moves. Understanding all processes behind hydraulic sorting is a prerequisite to correctly decipher the sedimentary history and the hydrodynamic power of the environment.

In the presented case study, the most prominent feature of the submarine part of the mid-Campanian Szozdy Delta System is the presence of tripartite cyclothems comprising, when complete, three units: from bottom to top, calcareous mudstone, calcareous sandstone, and calcareous gaize. The prevalent characteristics of the mineral assemblages analysed is the dominance of minerals belonging to the ZTR group (zircon, tourmaline, rutile), observed consistently across all units of the recognised cycles, irrespective of the analysed lithofacies.

An interesting recurring increase in tourmaline abundance, coupled with a simultaneous decrease in rutile abundance in one unit and the opposite situation in the other units of each cyclothem were observed. These relative changes are discussed as a consequence of hydraulic sorting, being the function of hydrodynamic power that existed during the deposition of the succeeding lithofacies.

The studied pair of minerals in several cases is one of the commonest in heavy mineral assemblages (also in the studied case). As being ultrastable components, tourmaline and rutile are common in sediments of various ages and environments, being resistant to even multiple recycling (Morton and Hallsworth 1994, 1999, 2007). Additionally, both these mineral phases are characterised by several interesting features: 1) both have high resistance to chemical and mechanical weathering (Hubert 1962; Garzanti 2017; Garzanti and Andò 2019) as well as are not impacted by burial diagenesis (e.g., Morton and Hallsworth 2007); as a result, in ancient sediments they retain a signature that is solely due to sedimentary processes; 2) in sediments, they usually take the form of well-rounded, egg-shaped grains or elongated self-shaped prisms (Mange and Maurer 1992); 3) they have markedly different densities: 4.23 g/cm^3 for rutile, 3.03-3.18 g/cm^3 for tourmaline (the latter density is for the dravite end-member); and 4) both minerals are very easily identifiable under the microscope (Mange and Maurer 1992).

The juxtaposition of the set of common and antagonistic physical characteristics of these two minerals, when joined together, justify, for the first time, the introduction of the rutile to tourmaline index (RuTidx), which is expressed by the equation:

$$RuTidx = \frac{rutile}{(toutmaline + rutile)} \times 100\ [\%]$$

The primary aim is to provide a straightforward description of the changes in the energy levels of sedimentary environments, particularly in clastic-dominated depositional systems, resulting from hydraulic sorting. In this case study, the RuTidx derived from the deltaic environment of the Late Cretaceous Szozdy Delta System (Remin *et al.* 2022a, b) is discussed. As derived from the recurrent changes of RuTidx, clear differences in the hydrodynamics of the environment might be interpreted in the recognised lithofacies. Accordingly, the relative increase in RuTidx should be understood as an increase in the energy of the sedimentary environment. The usefulness and limitations of RuTidx are additionally discussed.

PALAEOGEOGRAPHIC AND ENVIRONMENTAL CONTEXT OF THE SZOZDY DELTA SYSTEM

In the Late Cretaceous, central Europe was impacted by compressional tectonics, the results of which (i.e., basement uplift and inversion) are recorded across the entire Central European Basin

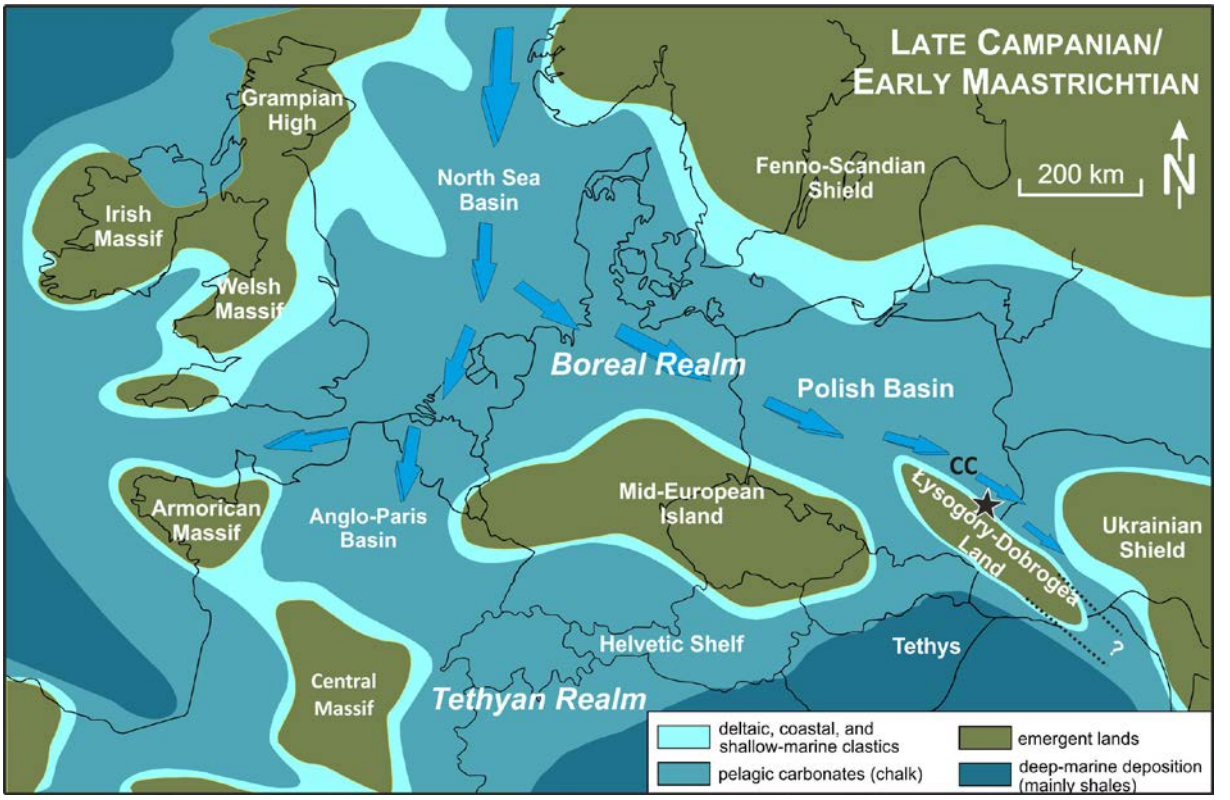

Text-fig. 1. Schematic palaeogeographic map for the Late Campanian/Early Maastrichtian (compiled from Ziegler 1990 and Dadlez *et al.* 1998) with the location of the studied section (marked with a black star) in SE Poland. Ocean currents (blue arrows) are based on Remin *et al.* (2016) and Remin (2018); the presence of contourite currents (CC) follows Krzywiec (2009) and Krzywiec *et al.* (2018); adapted from Remin *et al.* (2022a, b).

System. Material eroded from the uplifted structures was deposited in newly formed flexural basins (e.g., Ziegler 1990; Dadlez *et al.* 1995; Leszczyński and Dadlez 1999; Nielsen and Hansen 2000; Krzywiec 2006, 2009; Krzywiec and Stachowska 2016; Krzywiec *et al.* 2018; Kley and Voigt 2008; Voigt *et al.* 2021; Remin *et al.* 2022a, b). Late Cretaceous inversion tectonics also induced marked changes in palaeogeography and facies architecture, particularly in a belt along the margin of the East European Craton (Text-figs 1 and 2; e.g., Leszczyński 1997, 2010, 2012). In the Polish Cretaceous Basin, it is manifested by the transformation of the Mid-Polish Trough into the Mid-Polish Anticlinorium together with the formation of the Łysogóry-Dobrogea Land (Text-figs 1 and 2; for through review see Remin *et al.* 2022a, b).

The Roztocze Hills region

The Roztocze Hills form an elongated range of hills (approximately 25 × 185 km) between the cities of Kraśnik in southeast Poland and Lviv in western Ukraine (Text-fig. 2). They are located to the northeast and along the structurally elevated Mid-Polish Anticlinorium. To the southwest, the Roztocze Hills border the Carpathian Foredeep, filled by Miocene deposits, and the subsurface San Anticlinorium (the southeasternmost part of the Mid-Polish Anticlinorium; Text-fig. 2).

The Roztocze Hills are mainly built of the Campanian (c. 550 m thick) and incomplete Maastrichtian (c. 250 m) deposits that dip gently to the northeast. Older rocks are not exposed in this area. Being located in the proximity of the recent Mid-Polish Anticlinorium, which formed an elevated Łysogóry-Dobrogea Land during the Late Cretaceous, the Roztocze Hills enable access to various facies: calcareous sandstones, calcareous mudstones, argillaceous mudstones or clays, various opoka facies (siliceous chalk/limestones with a variable admixture of biogenic silica), and gaizes (siliceous limestones with a considerable admixture of detrital quartz, glaucony, and clay) (for a full account see Remin *et al.* 2022a, b).

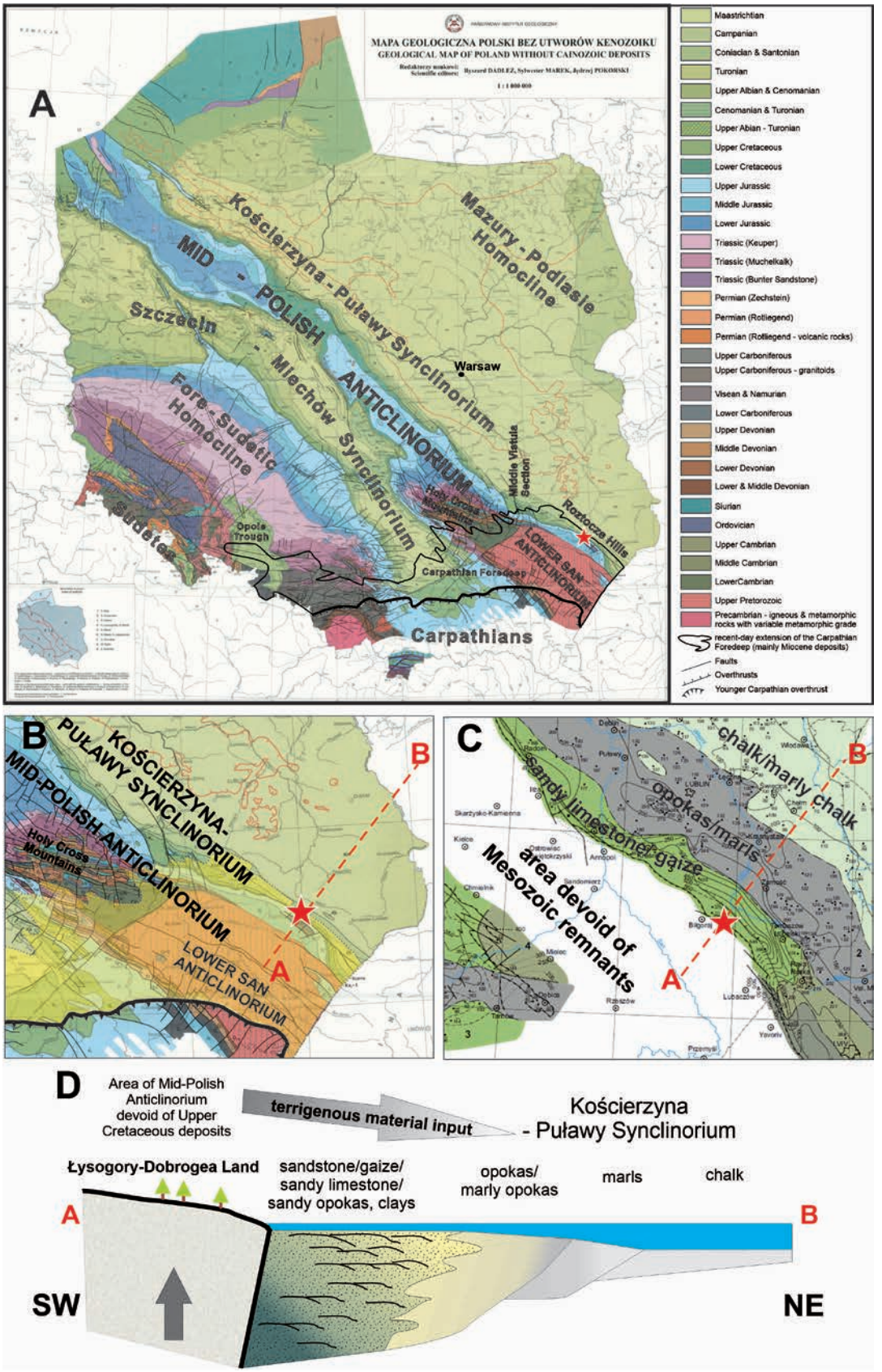
A
MAPA GEOLOGICZNA POLSKI BEZ UTWORÓW KENOZOIKU
GEOLOGICAL MAP OF POLAND WITHOUT CAINOZOIC DEPOSITS
Mazury - Podlasie Homocline
Kościerzyna - Puławy Synclinorium
MID - POLISH ANTICLINORIUM
Szczecin - Miechów Synclinorium
Fore-Sudetic Homocline
Sudetes
Opole Trough
Warsaw
Middle Vistula Section
Holy Cross Mountains
Roztocze Hills
LOWER SAN ANTICLINORIUM
Carpathian Foredeep
Carpathians
Maastrichtian
Campanian
Coniacian & Santonian
Turonian
Upper Albian & Cenomanian
Cenomanian & Turonian
Upper Albian - Turonian
Upper Cretaceous
Lower Cretaceous
Upper Jurassic
Middle Jurassic
Lower Jurassic
Triassic (Keuper)
Triassic (Muschelkalk)
Triassic (Bunter Sandstone)
Permian (Zechstein)
Permian (Rotliegend)
Permian (Rotliegend - volcanic rocks)
Upper Carboniferous
Upper Carboniferous - granitoids
Visean & Namurian
Lower Carboniferous
Upper Devonian
Middle Devonian
Lower Devonian
Lower & Middle Devonian
Silurian
Ordovician
Upper Cambrian
Middle Cambrian
LowerCambrian
Upper Pretorozoic
Precambrian - igneous & metamorphic rocks with variable metamorphic grade
recent-day extension of the Carpathian Foredeep (mainly Miocene deposits)
Faults
Overthrusts
Younger Carpathian overthrust
B
KOŚCIERZYNA-PUŁAWY SYNCLINORIUM
MID-POLISH ANTICLINORIUM
Holy Cross Mountains
LOWER SAN ANTICLINORIUM
A
B
C
chalk/marly chalk
opokas/marls
sandy limestone/gaize
area devoid of Mesozoic remnants
D
Area of Mid-Polish Anticlinorium devoid of Upper Cretaceous deposits
terrigenous material input
Kościerzyna - Puławy Synclinorium
Łysogory-Dobrogea Land
sandstone/gaize/ sandy limestone/ sandy opokas, clays
opokas/ marly opokas
marls
chalk
SW
NE

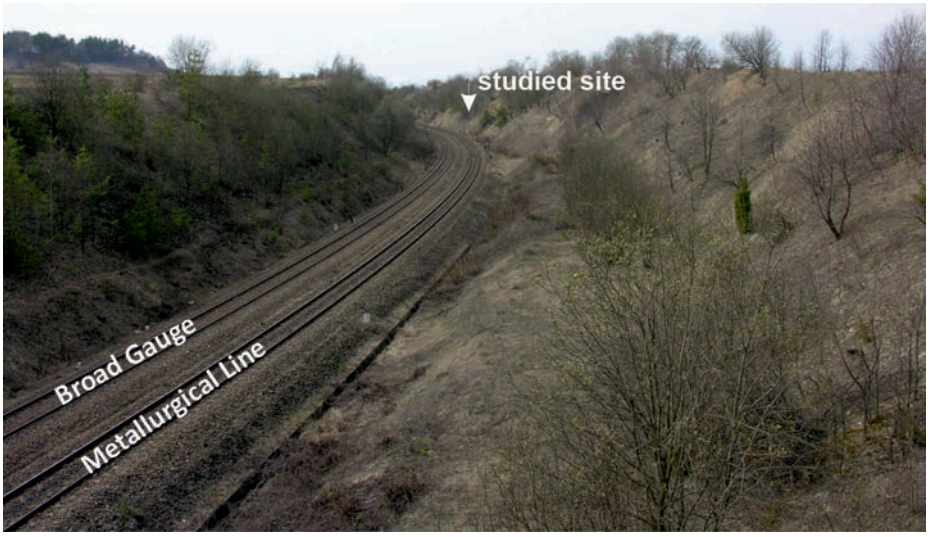

Text-fig. 3. General view of the Szozdy section. The exposures extend along both sides of the railroad cut over a distance of ~800 m.

The Szozdy section

The Szozdy section is situated in a railroad cut of the Broad Gauge Metallurgical Railway Line (Text-fig. 3), southwest of Zwierzyniec town and close to the small village of Szozdy in southeast Poland. The fossil assemblage is indicative of a mid-Campanian age (Remin *et al.* 2015a, b, 2022a, b). Notably, plant debris is relatively common, including complete compound leaves in addition to partially carbonised imprints of leaves and boughs or branches.

The interval available at Szozdy, together with other sections in the Roztocze Hills (Remin *et al.* 2015b, 2022a, b), is easily correlatable with the equivalent interval in the Middle Vistula River Valley composite section (e.g., Walaszczyk 2004; Walaszczyk *et al.* 2016; Text-fig. 4), and other sections of the southeastern Polish Cretaceous Basin (Remin *et al.* 2022b) enabling comparison of different sedimentary environments.

The total thickness of the Szozdy Delta System cannot be estimated (Remin *et al.* 2022a, b) since neither the lower nor the upper limit of the cyclic succession is known. The exposure at Szozdy (Text-fig. 3) gives access to ~30-35 m of the succession over a lateral distance of ~800 m. Other data, such as exposures or well-logs, are not available, precluding any firm conclusions. In the present study, heavy mineral assemblages were collected from a ~12 m-thick interval, consisting of six cycles, both complete (III to VI) and incomplete (e.g., II; Text-fig. 5).

The presence of tripartite cyclothems constitutes the most distinct feature of the Szozdy section. A cyclothem, when complete, consists of three units: calcareous mudstone > calcareous sandstone > calcareous gaize (Text-fig. 5) referred further to as mudstones, sandstones, and gaize. The full characteristics of the succeeding lithofacies of the Szozdy Delta System was provided recently by Remin *et al.* (2022a, b) together with data on facies, bathymetry, and sedimentology, therefore the reader is kindly referred to those papers for further details. As such, only short descriptions are provided below.

The mudstone lithofacies (Text-fig. 5) is dark grey and poorly indurated. The colour is most likely derived from disseminated carbonised organic matter. The clay and silt content is highest within the whole section of studied cyclothems. It was assigned to a prodelta environment (Remin *et al.* 2022a).

The sandstone lithofacies (Text-fig. 5) is yellow to yellow-brownish and poorly indurated. The clay and silt content is ~10% lower than in the underlying

← Text-fig. 2. Geological setting of the study area. A – Location (marked with a red star) on the geological map of extra-Carpathian Poland, excluding Cenozoic deposits, except for the modern extension of the Carpathian Foredeep; adapted from Dadlez *et al.* (2000); tectonic units after Żelaźniewicz *et al.* (2011); B – Detailed map, relative to the position of the Holy Cross Mountains (HCM) and the Lower San Anticlinorium; C – General distribution of Campanian lithofacies in SE Poland (adapted from Świdrowska 2007); D – Depositional, structural, and environmental interpretation of facies and bathymetry in a cross-section perpendicular to the axis of the Mid-Polish Anticlinorium (adapted from: Walaszczyk and Remin 2015; Remin *et al.* 2015a, 2022a, b).

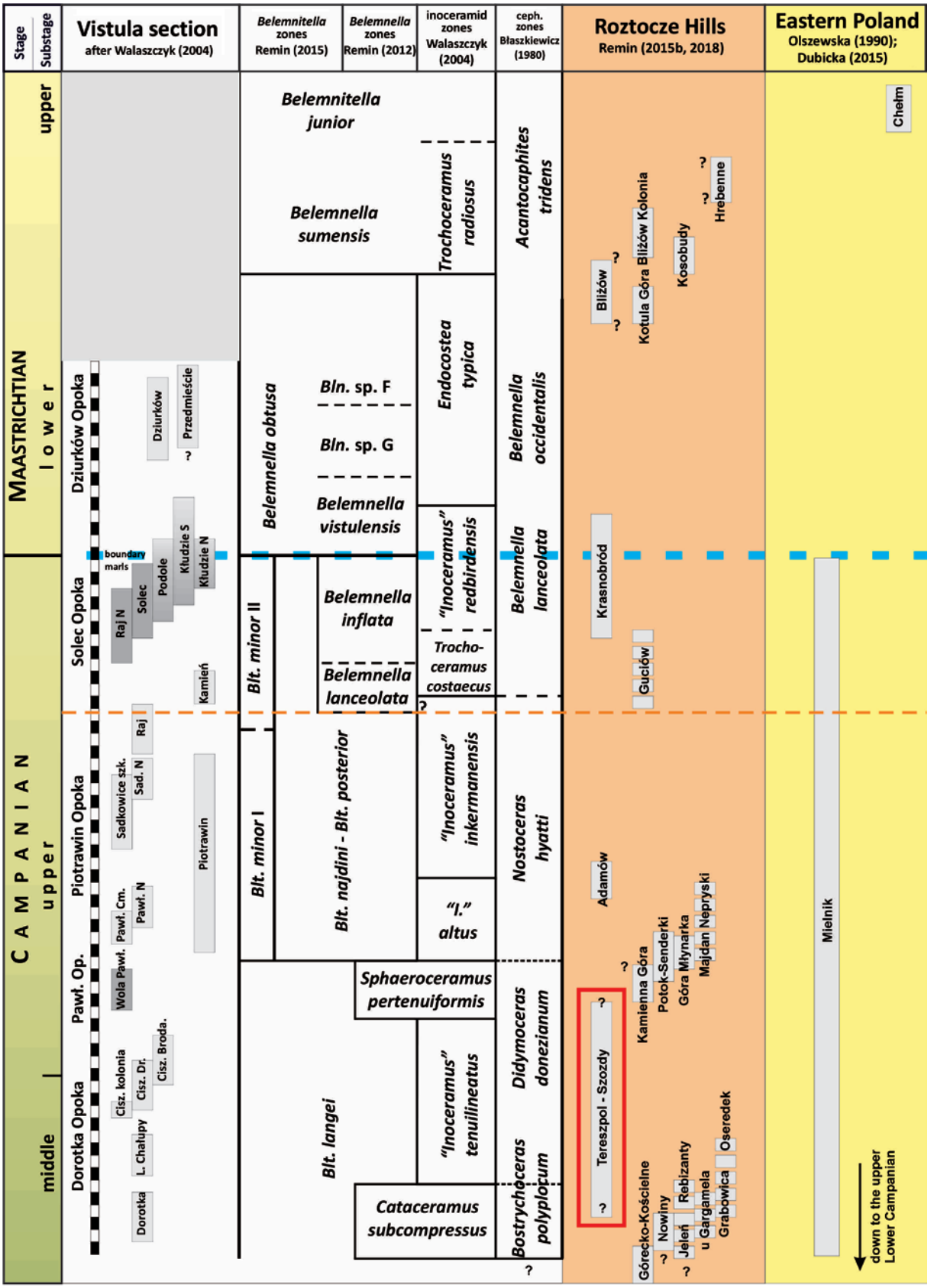
Stage
Substage
Vistula section
after Walaszczyk (2004)
Belemnitella zones
Remin (2015)
Belemnella zones
Remin (2012)
inoceramid zones
Walaszczyk (2004)
ceph. zones
Błaszkiewicz (1980)
Roztocze Hills
Remin (2015b, 2018)
Eastern Poland
Olszewska (1990); Dubicka (2015)
MAASTRICHTIAN
lower
upper
CAMPANIAN
upper
middle
Dorotka Opoka
Pawł. Op.
Piotrawin Opoka
Solec Opoka
Dziurków Opoka
boundary marls
Dorotka
L. Chałupy
Cisz. kolonia
Cisz. Df.
Cisz. Broda.
Wola Pawł.
Pawł. Cm.
Pawł. N
Sadkowice szk.
Sad. N
Raj
Piotrawin
Raj N
Solec
Podole
Kludzie S
Kludzie N
Kamień
Dziurków
Przedmieście
Belemnitella junior
Belemnella sumensis
Belemnella obtusa
Belemnella vistulensis
Belemnella inflata
Belemnella lanceolata
Bln. sp. F
Bln. sp. G
Blt. minor II
Blt. minor I
Blt. najdini - Blt. posterior
Blt. langei
Trochoceramus radiosus
Endocostea typica
"Inoceramus" redbirdensis
Trocho-ceramus costaecus
"Inoceramus" inkermanensis
"I." altus
Sphaeroceramus pertenuiformis
"Inoceramus" tenuilineatus
Cataceramus subcompressus
Acantocaphites tridens
Belemnella occidentalis
Belemnella lanceolata
Nostoceras hyatti
Didymoceras donezianum
Bostrychoceras polyplocum
Bliżów
Kotula Góra Bliżów Kolonia
Kosobudy
Hrebenne
Krasnobród
Guciów
Adamów
Tereszpol - Szozdy
Kamienna Góra
Potok-Senderki
Góra Młynarka
Majdan Nepryski
Górecko-Kościelne
Nowiny
Jeleń
Rebizanty
u Gargamela
Grabowica
Oseredek
Chełm
Mielnik
down to the upper Lower Campanian

Sample/mineral	Garnet	Kyanite	Rutile	Sillimanite	Staurolite	Tourmaline	Zircon	Others	Total grains counted
Sz1	31	21	22	1	19	127	68	13	302
Sz3	24	34	26	4	47	138	42	23	338
Sz4	12	6	14	0	24	112	83	14	265
Sz5	4	6	6	0	2	41	20	4	83
Sz6	12	37	27	8	24	93	24	5	230
Sz7	14	32	40	2	14	88	37	3	230
Sz8	22	30	47	10	20	76	22	6	233
Sz9	28	22	49	14	22	69	18	0	222
Sz10	33	36	70	28	30	134	63	5	399
Sz11	28	36	16	28	32	103	36	0	279
Sz12	22	20	30	30	25	217	51	5	400
Sz13	43	32	24	12	38	145	55	2	351
Sz14	16	29	40	27	26	176	46	3	363
Sz16	26	42	79	16	44	135	56	2	400
Sz17	35	68	80	8	36	141	29	0	397

Table 1. Results of point counting of the number of particular minerals in succeeding samples.

mudstone. The sand fraction, mainly consisting of quartz, is proportionally the highest of the lithofacies recognised in the Szozdy section. The quartz sand is still fine-grained; however, grain sizes range up to ~0.25 mm, twice as large as in the underlying calcareous mudstones. It was assigned to a delta lobe environment, relatively close to the river discharge (Remin *et al.* 2022a).

The gaize lithofacies is white-grey and fully indurated; in the field, it is expressed as protruding horizons between more erosion-prone deposits (Text-fig. 5). This unit contains a limited clay and silt fraction. The $CaCO_3$ content is the highest among the recognised lithofacies (up to 75%). It was assigned to an environment cut off from terrigenous-sourced material, but still in close proximity to land (Remin *et al.* 2022a).

MATERIAL AND METHODS

Twenty-two samples were collected for heavy minerals analysis from the Szozdy section (Text-fig. 5); seventeen covering the lower three cyclothems (two complete III and IV and one incomplete II) were further processed in the analysis. Two samples (no. 2 and no. 15 in Text-fig. 5) were eliminated from further consideration because of the dominance of pyrite grains.

Firstly, the samples were mechanically crumbled into fragments 1–3 cm in size. Subsequently, to prevent individual grains from crushing by multiple hammering, liquid nitrogen methods were used for rock disintegration, as proposed initially for foraminifera extraction by Remin *et al.* (2012). This method ensures preservation of the original shape.

The obtained residues were treated with 10% acetic acid to dissolve $CaCO_3$. Terrigenous material was further processed in an ultrasonic cleaner to remove grain coatings, e.g., clay and Fe-oxides and other unwelcome particles. Subsequently, samples were sieved to obtain the 63–250 μm fraction. Heavy minerals were then separated by centrifugation in a sodium poly-tungstate solution (~3.0 g/cm^3) and recovered by partial freezing with liquid nitrogen.

The obtained heavy minerals were immersed in Canada Balsam and examined using a polarizing microscope. To determine the relative abundance of heavy minerals in a sample, the ribbon condition was used (Galehouse 1971). This technique involves randomly selecting ribbons (bands) within the microscope slide. Along the randomly selected ribbons, by point counting, up to 400 specimens in total in each studied sample were counted including different mineral phases (compare Table 1). During the analysis, focus was mainly on the number of grains of individual minerals. Only in one case (sample Sz5; Table 1) the counts did not reach the standard requirements.

← Text-fig. 4. Stratigraphic position of the Szozdy section (red rectangle marks the known stratigraphic extension of the section) in relation to the Middle Vistula Valley section (left column in white; the metre-scale is valid only for this section; scale bar = 2 m); Roztocze Hills area (middle column in orange); Eastern Poland (right column in yellow). The biostratigraphic subdivision follows Błaszkiewicz (1980), Walaszczyk (2004), Remin (2012, 2015, 2018), and Remin *et al.* (2015b, 2022a, b); figure adapted from Remin *et al.* (2022b). The Campanian/Maastrichtian boundary based on the GSSP Tercis definition (Odin and Laumurelle 2001) is marked with a thick blue dashed line, based on belemnites (e.g., Christensen 1997) is marked with a thin orange dashed line.

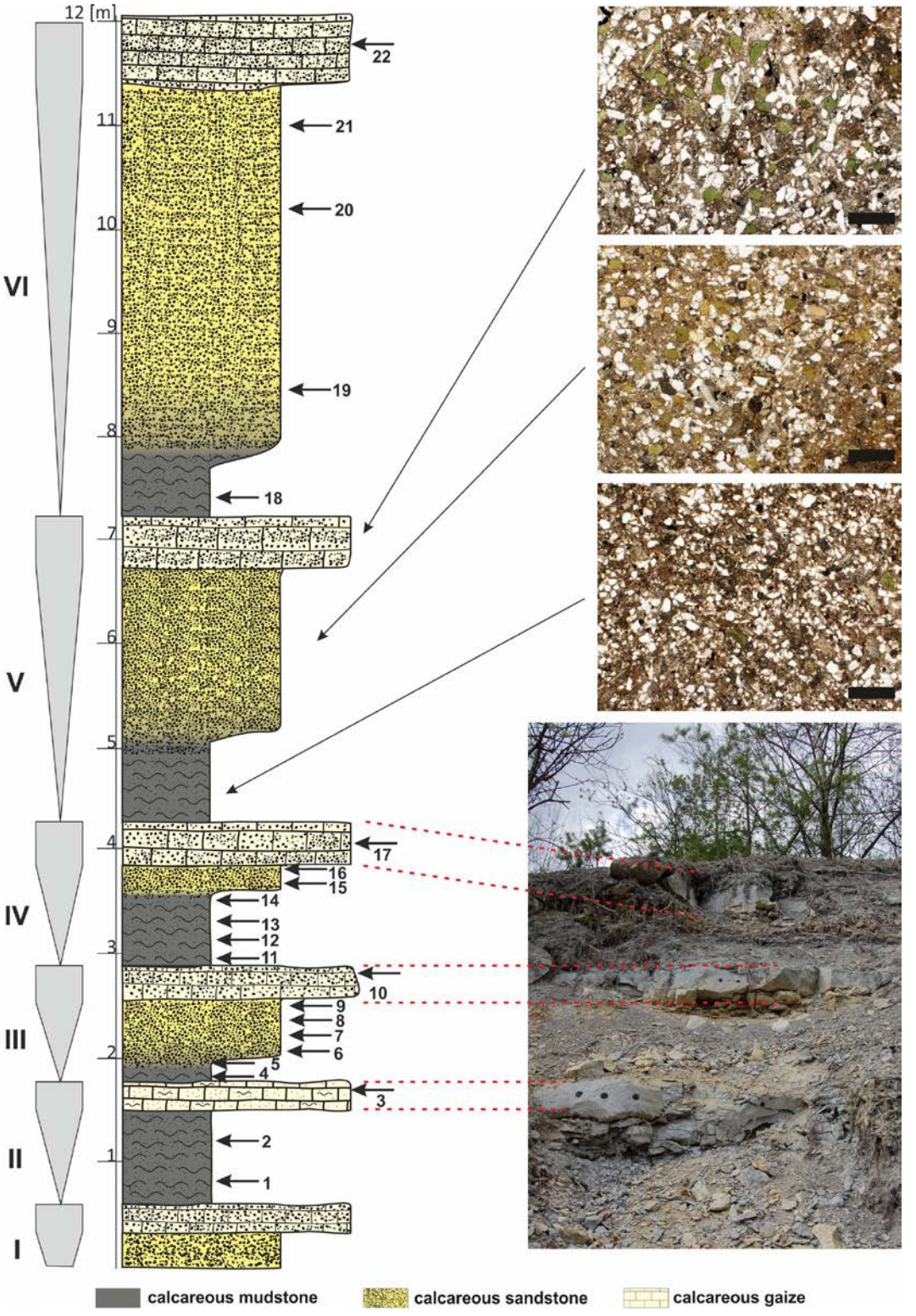

Text-fig. 5. Lithological column of the Szozdy section (adapted from Remin *et al.* 2022a). The left side column (grey) indicates coarsening-upward cyclothems marked with Roman numerals. Top right: typical thin sections from successive lithofacies of a single cyclothem; scale bar = 500 μm; most white particles represent quartz grains. Bottom right: field photo of a part of the succession with prominent calcareous gaize layers, indicated on the section by red dashed lines. The horizontal scale in the log represents the relative resistance of particular units to weathering. Arrows with numbers indicate the collected samples.

However, the relative proportions of less common minerals are sometimes difficult to assess without proper statistics, and their variation might be distorted. Such difficulties might be easily overcome by calculating standardised Z-scores for each mineral species and plotting them against stratigraphic intervals. This standardised Z-score statistics quantifies how many standard deviations each sample is from the mean value for the whole group for the entire Szozdy section; they were calculated according to the formula:

$$score_{i,z} = \frac{x_{i,z} - mean_i}{sdev_i}$$

where $X_{i,z}$ = individual mineral count for the *i*-th mineral at stratigraphic level z; $mean_i$ = mean mineral percentage for species *i*; and $sdev_i$ = standard deviation for species *i*.

Principal Component Analysis (Hammer and Harper 2006) was applied to group the recognised lithotypes to a particular sedimentary environment – proximal or distal, thus characterised by different hydrodynamic power.

Additionally, R Codes were provided for the prediction of: 1) the flow stress τ that is required for entrainment of a grain of a certain diameter (values calculated based on Komar and Wang 1984; see Appendix 1), and 2) the prediction of the relationship between settling velocity and grain diameter for rutile, tourmaline, and quartz (values calculated based on Ferguson and Church 2004; see Appendix 2).

PHYSICAL FUNDAMENTALS OF GRAIN TRANSPORT PROCESSES

Hydraulic sorting

The basic processes that determine hydraulic sorting are transport type, i.e., bedload (saltation and rolling and crippling) or in the water column (in the suspension), selective entrainment, and settling velocity. All of them are directly related to flow velocity, density, diameter and shape of grains, and kinematic viscosity of the medium in which particle movement occurs (e.g., Cascalho and Fradique 2007). Therefore, all these factors should be considered simultaneously.

Heavy mineral sorting is supported by several examples both in the geological record and in recent environments (e.g., Komar and Wang 1984; Morton and Hallsworth 1994, 1999, 2007; Cascalho and Fradique 2007; Frihy 2007; Garzanti 2017; Nauton-Fourteu *et al.* 2021). As an example, we provide along-profile

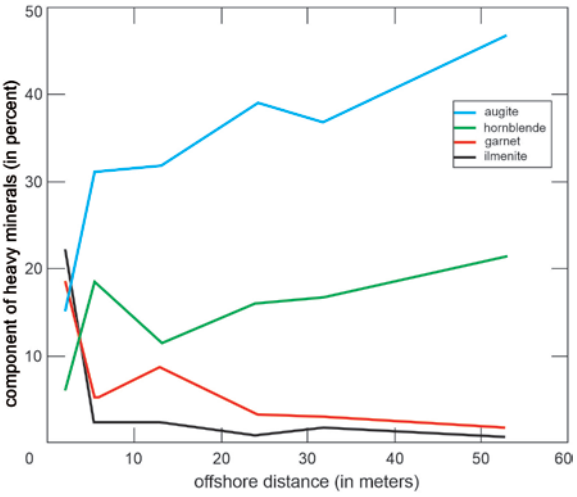

Text-fig. 6. Changes in the percentage of heavy minerals across the beach (after Komar and Wang 1984).

variations in heavy-mineral percentages in the swash zone of an Oregon beach (Komar and Wang 1984; Text-fig. 6). In this case, nearly all of the very dense minerals like ilmenite and garnet occupied the area of the beach – their concentration decreased rapidly in the offshore direction even on a relatively short distance. On the contrary, the concentration of the less dense hornblende and augite increased markedly toward the offshore zone (Text-fig. 6).

Selective entrainment

Crucial for selective entrainment is the grain mobility, which mainly depends on the exposure to water flow and on the pivoting angle of the grains (Komar and Wang 1984; Text-fig. 7). The shear force associated with the flow velocity falls toward the bottom due to frictional force. Consequently, larger grains protruding above the bottom are at greater risk of entrainment. The second element, i.e., the pivoting angle of the grain (Miller and Byrne 1966), depends on the ratio between the diameter of the grain (which is going to be entrained) in comparison to the average diameter of grains on the bottom. In addition, it depends on the grain roundness and shape, and sorting effects (see Text-fig. 7).

Modelling selective grain entrainment explains the observed patterns of mineral variations on beach placers (Text-figs 7 and 8). The model introduced by Komar and Wang (1984) enables to determine the shear force required to entrain (move) a grain with a certain diameter. According to this model,

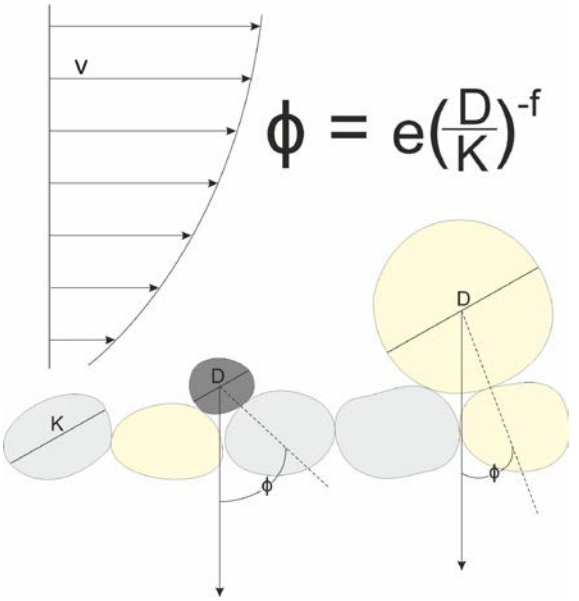

Text-fig. 7. Parameters used to describe the pivoting angle F: e – parameter incorporating the effects of shape and roundness in both particle and bed (e = 50 for spheres, e = 61.5 for intermediate roundness, e = 70 for low roundness); f – parameter incorporating the effects of sorting of the bed grains (f = 0.3, a constant value); D/K – ratio of the diameter of a single grain to the average diameter of the grains on the bottom, where K = 0.290 mm (based on Komar and Wang 1984); V – local average velocity of water within the turbulent flow; this average increasing with distance above the sediment (adapted from Komar 2007).

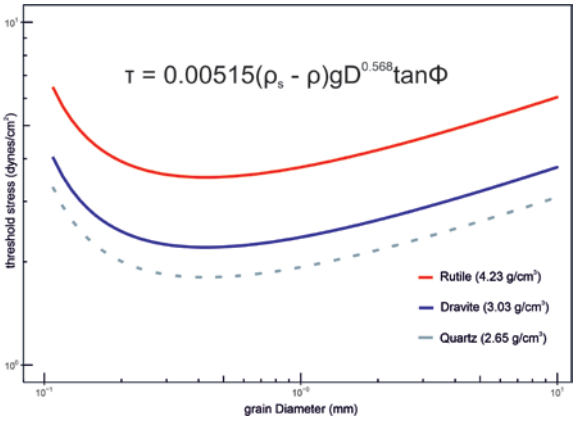

Text-fig. 8. Calculated curves for rutile, tourmaline and quartz showing the flow stress τ that is required to threshold or entrain a grain of diameter D. For D < 0.1 cm; ϱ_s = density of mineral; ϱ = density of water; g = acceleration due to gravity; tanΦ = tangent of the pivote angle (compare Text-fig. 7). See Appendix 1 for R Code used in the calculations.

picking up grains smaller than 100 μm from the bottom requires the same shear force as picking up grains a hundred times larger (see Text-fig. 8). This is related to the pivoting angle – the smaller the grain, the greater the pivoting angle making their entrainment more challenging (e.g., Miller and Byrne 1966). Grains of the medium sand fraction are preferred for transport because of the balanced ratio of the pivoting angle to their diameter (Miller and Byrne 1966; Text-fig. 8).

Settling velocity

Another key aspect responsible for hydraulic sorting is the grain settling velocity. Grains for which the particle Reynolds number (Re = wD/v; symbols described below) exceeds 1 are not subject to laminar motion. Turbulent drag begins to dominate as a result of the sinking of grains, which is caused by the high difference in pressure at the front and back of the falling grain – the larger pressure is at the bottom, the smaller pressure is on the top of the falling grain. For larger grains, the viscosity drag of the medium has a negligible effect on the settling velocity. Attempts to describe turbulent motion have been the subject of many studies (e.g., Yalin 1972; Hallermeier 1981; Dietrich 1982; Cheng 1997; Ahrens 2000). In simple words, the model proposed by Ferguson and Church (2004) allows to extend Stokes' law to grains exceeding particle Reynolds number >1 based on the following equation (see Text-fig. 9):

$$w = \frac{RgD^2}{C_1 v + (0.75 C_2 RgD^3)^{0.5}}$$

where: w – particle's fall velocity, D – diameter, R – submerged specific gravity (1.65 for quartz in water), g – acceleration due to gravity, v – kinematic viscosity of the fluid ($1.0'10^{-6}$ kg $m^{-1}s^{-1}$), C_1 and C_2 – constants that take values: 18 and 0.4 for smooth spheres, for typical natural sands these parameters take values 18 and 1.0, and a likely limit for very angular grains are: 24 and 1.2.

The equation of Ferguson and Church (2004) contains only two coefficients: the first (C_1) is constant in Stokes' equation for laminar settling; the second (C_2) is the constant drag coefficient for particle Reynolds number not exceeding 10^3 ($1 < Re < 10^3$), which corresponds to about 0.1 < D < 4 mm for quartz sand settling in water.

RESULTS AND DISCUSSION

The heavy mineral assemblages within the Szozdy Delta System exhibit small differentiation and maintain a consistent composition. The analysed associations encompass ultrastable phases, prom-

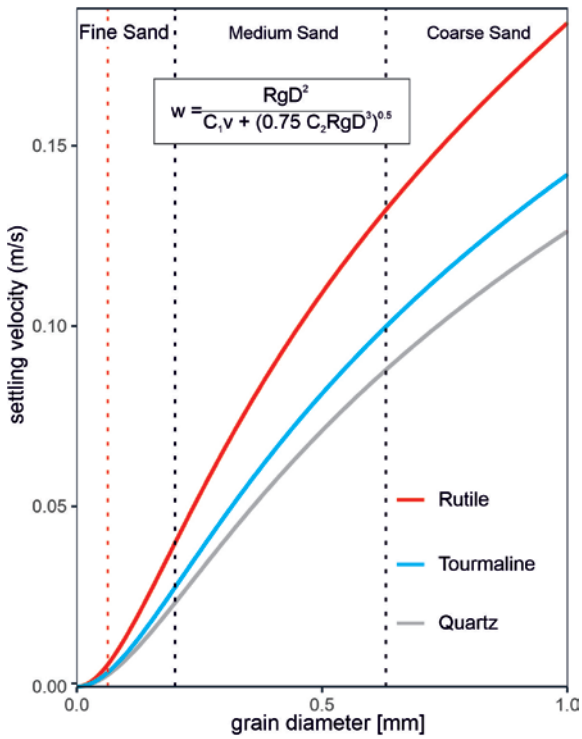

Text-fig. 9. Predicted relationship between settling velocity and grain diameter for rutile, tourmaline, and quartz (C_1 = 18 and C_2 = 1); the values on the chart were calculated based on the equation of Ferguson and Church (2004) as shown in the figure. See Appendix 2 for R Code used in the calculations.

inently featuring zircons, tourmalines, and rutiles (ZTR group), as well as stable phases like garnet, kyanite, staurolite, and other subordinate species, including sillimanite, chlorite, Cr-spinel, epidote, and single apatite grains (Table 1).

The zircon-tourmaline-rutile (ZTR) maturity index (Hubert 1962) ranges between 55-80% (mean = 67%). The highest ZTR values are associated with the calcareous mudstone lithofacies, which are dominated by tourmaline grains (Text-fig. 8). The GZi provenance-sensitive index (Morton and Hallsworth 1994) exhibits values between 10 and 60%. A full account of the heavy mineral assemblages from the Szozdy section will be provided in a future paper (Cyglicki and Remin submitted).

Tourmalines predominate within the examined heavy mineral assemblages. They constitute a minimum of one-third (31%), and in some cases, as much as half (54%) of the assemblages. Notably, their abundance demonstrates a positive correlation with the calcareous mudstone lithofacies. The rutile content within these assemblages ranges from 5% to 22%. There is an observable increase in rutile concentration in sandy lithofacies (Text-fig. 10). Both mineral phases are dominated by the angular to subrounded grains and counts for tourmaline c. 80% and for rutile c. 65-70% (compare Text-fig. 10).

To emphasise the relative changes in abundance of these two mineral species, a standardised Z-score statistic was calculated (Text-fig. 11; see Ryan *et al.* 2007 for comparison). Distinct changes of the rutile and tourmaline abundance pattern is observed in the recognised lithofacies, i.e., these two mineral phases are inversely correlated (Text-fig. 11).

In the mudstone unit of cyclothem III, the abundance of the tourmaline content is significantly higher than average (up to 1.5 standard deviations), whereas rutile is markedly reduced (by similar values; compare Text-fig. 11). In the sandstone unit of cyclothem III, the trend is opposite – the rutile abundance is markedly elevated (up to c. ~2.0 standard deviations), while the tourmaline content is c. ~1.5 standard deviations lower than average (Text-fig. 11). A similar pattern is observed in the other corresponding units.

A different, and at first glance contradictory, pattern is observed for the calcareous gaize lithofacies (Text-figs 11 and 12). The trend of rutile – tourmaline abundance in gaize always repeats the pattern observed in the underlying unit. This phenomenon is well observable, especially in the incomplete cyclothems (compare the top of cycle II; Text-figs 11 and 12), in which the sandy unit is not present; in this case, gaize lies directly on the muddy unit and repeats its mineral composition (compare also Remin *et al.* 2022a). The same is true for the gaize that lies over

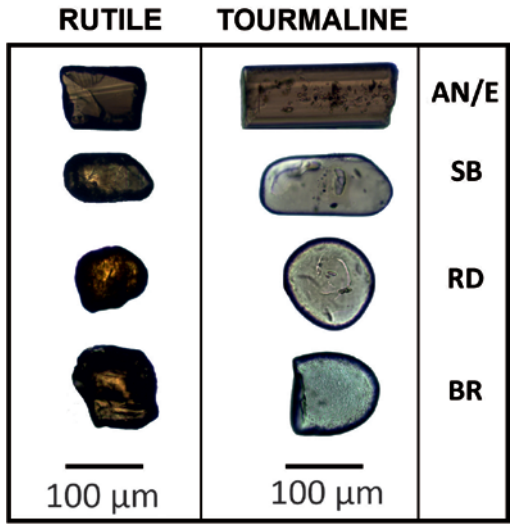

Text-fig. 10. Exemplary degree of roundness of the analysed rutile and tourmalines.

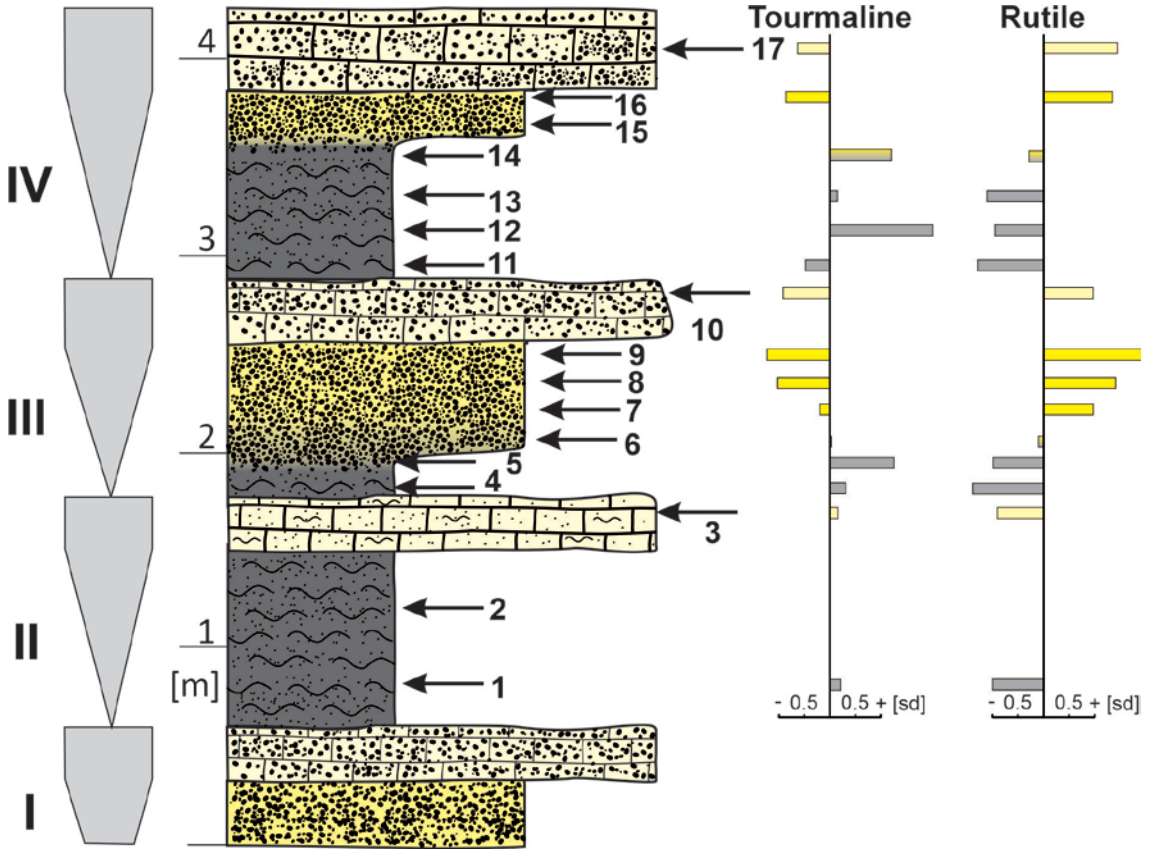

Text-fig. 11. Vertical chart of Z-score standardised rutile and tourmaline abundance in the Szozdy section. The vertical line in each case represents the mean abundance of the analysed minerals over the whole section. The bars are associated with the samples shown in the lithological column; sd – standard deviation. The cycles are marked with Roman numerals (compare Text-fig. 5); arrows with numbers indicate the collected samples; the colours of the bars correspond to the colours of the particular lithofacies.

the sandy unit where the pattern follows the mineral composition of the sandstone lithofacies (e.g., the top of cyclothem III and others if complete; Text-fig. 11).

The succeeding units of the cyclothems were interpreted to be deltaic in origin, representing the submarine part of the delta (up to now the delta plains have not been recognised; see Remin *et al.* 2022a). Accordingly, the muddy unit represents the most distal lithofacies occupying the position of the prodelta or an analogous environment. The sandy lithofacies were deposited in a more proximal position to the main source area (e.g., close to the river discharge; close to the land; Text-figs 12 and 13). A special case is the gaize lithofacies which seems to be a unit with, at least in part, a diagenetic overprint. It is interpreted to have originated during the stoppage of the detrital material supply which allows the calcification of the upper portion of the underlying unit (mudstone or sandstone), therefore the gaize units repeat their textural and mineral composition (RuT index, grain size and roundness; Remin *et al.* 2022a) both in complete and incomplete cyclothems (i.e., muddy and sandy facies; Text-fig. 11).

This pattern is also underlined by PCA analysis based on the abundance of rutile and tourmaline (Text-fig. 12). In this analysis four groups were recognised depending on their position in the stratigraphic column understood as representing different sedimentary environments of different energy. In the plot the muddy lithofacies occupy a distal position whereas the sandy lithofacies hold the proximal one (Text-fig. 12). The samples from the muddy to the sandy transitional interval (compare Text-fig. 11) were grouped in-between the proximal and distal lithofacies (Text-fig. 12). Similarly, as mentioned above, the gaize lithofacies was classified both in proximal and distal positions (depending on whether they represent complete or incomplete cycles) holding the same distance/energy environment as the underlying unit (Text-fig. 12).

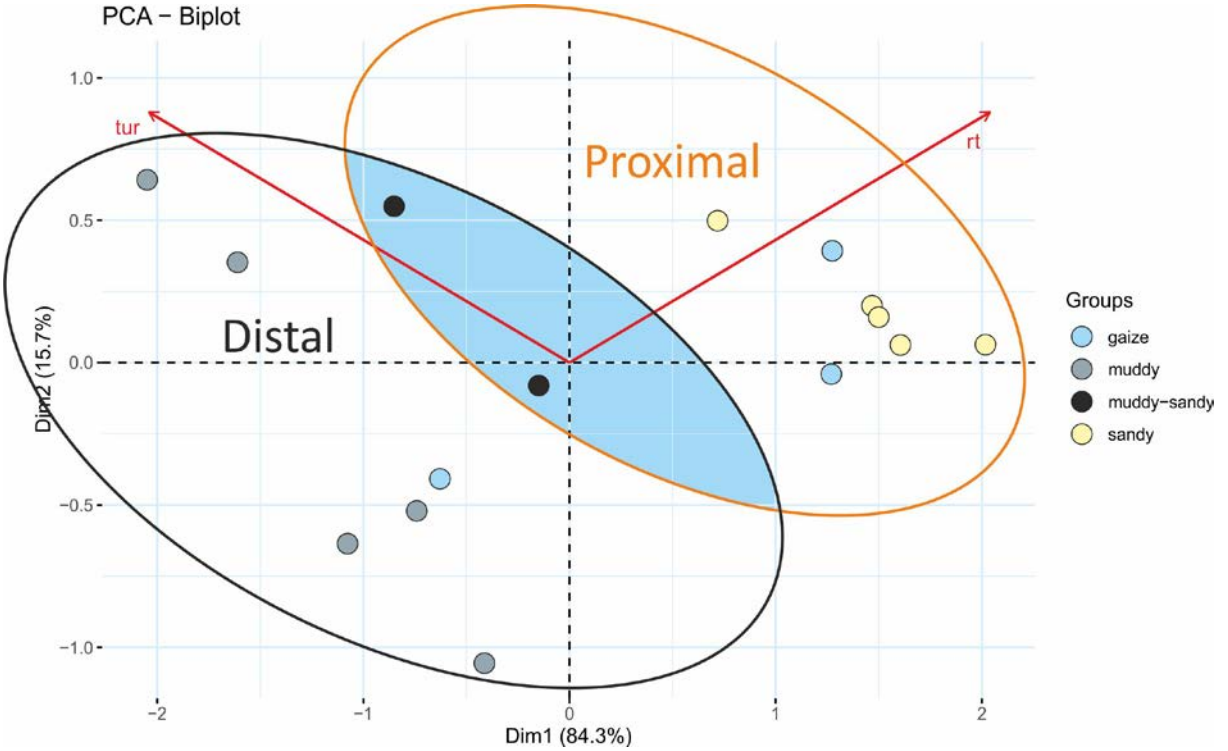

Text-fig. 12. PCA division of samples from the succeeding lithofacies based on rutile (rt) and tourmaline (tur) abundance in the Szozdy section interpreted to be in a proximal, distal and intermediate position in relation to land area.

The physical and chemical properties of rutile and tourmaline make them ideal candidates for interpreting hydraulic sorting, especially in the ancient sediments, and by extension – the hydrodynamic power in the sedimentary environment.

Although processes behind hydraulic sorting can often completely change the nature of the heavy mineral suite, especially when the hydrodynamic power changes, e.g., in nearshore-offshore environments (e.g., Komar and Wang 1984; Text-fig. 6) or within deltaic systems, the recognised RuTidx pattern can be fully explained on the basis on physical fundamentals elaborated above.

Rutile and tourmaline grains are characterised by high resistance to chemical and physical weathering conditions, therefore by studying these mineral phases we are sure that we are referring almost exclusively to hydraulic processes. The passage of tourmaline and rutile through successive sedimentary-diastrophic cycles results in a unification of their shape (egg-shape), which is of primary importance in hydraulic sorting. In the discussed case, the longest diameter of both mineral phases falls within the range of 90-170 mm (median = 130) for rutile grains and 100-250 mm (median = 150) for tourmaline grains, independently of the host lithofacies (succeeding units of the cyclothem), however, they are characterised by significant different densities (4.23 and 3.03-3.18 respectively for rutile and tourmaline–dravite end-members in this case), which makes them hydraulic-sensitive.

Because of different physical properties, both mineral phases will be subjected to different transportation processes and selective entrainment. According to Komar and Wang (1984), the share force associated with the flow velocity falls toward the bottom because of frictional force (Text-fig. 7). Additionally, the calculated curves for rutile, tourmaline and quartz (for the purpose of this article; Text-fig. 8) show that the flow stress that is required to threshold or entrain a grain of known diameter will be much higher for rutile (Text-fig. 8). As shown in Text-fig. 8 the share force required to pick up the rutile grains needs several times more energy because of its markedly higher density and smaller diameter. Consequently, by similar shape (egg-shape) of rutile and tourmaline, the lighter and larger tourmaline grains, additionally favoured by a smaller pivoting angle (Text-figs 7 and

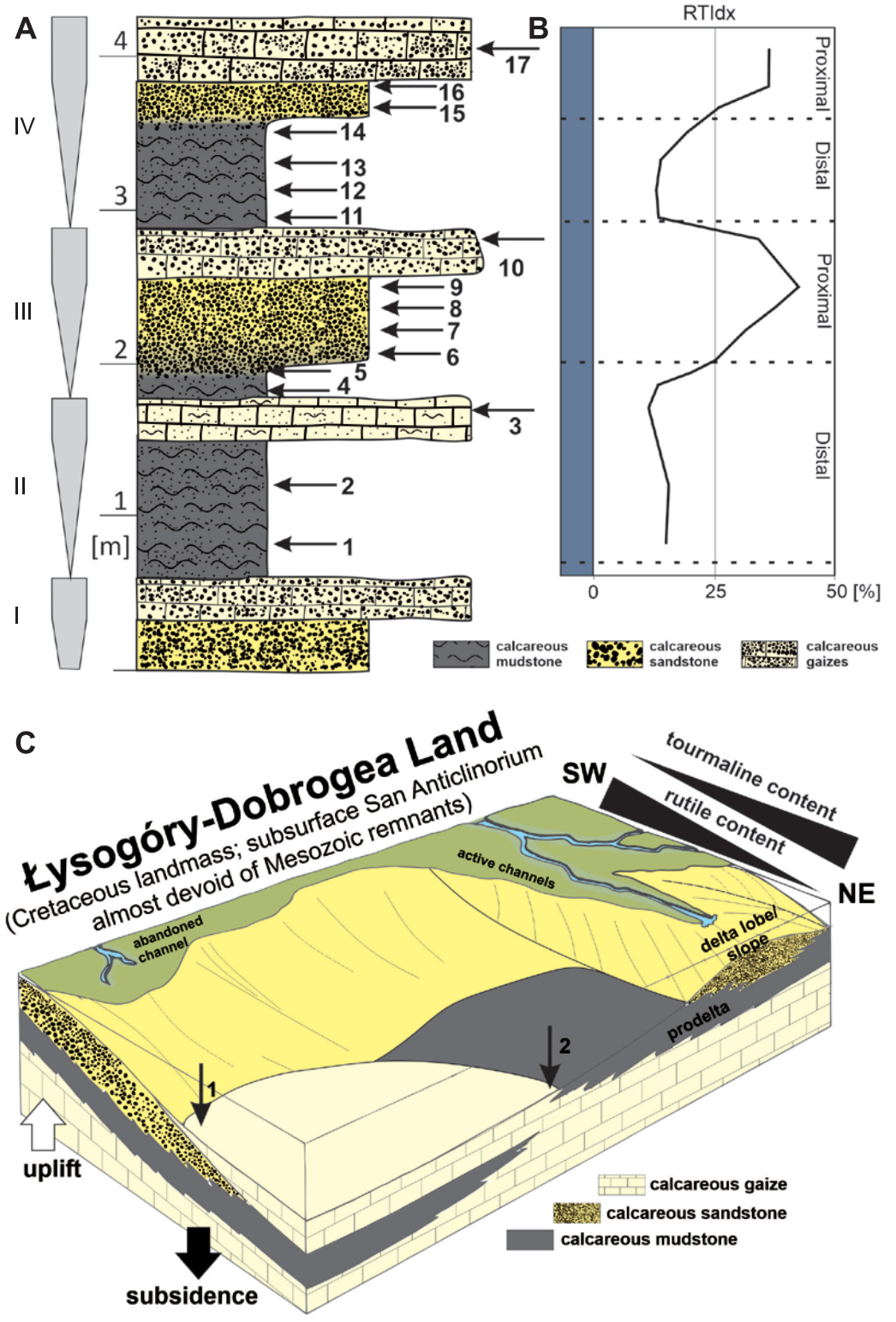

Text-fig. 13. Lithological log of the analysed cyclothems (A) with the curve (B) providing the environmental interpretation based on the RuT index. The block diagram (C) illustrates the relationships between the subaerial (beyond the study area) and subaqueous deltaic environments of the Szozdy Delta System in relation to active and abandoned distributary channels. Arrows 1 and 2 indicate two different situations, i.e., a full tripartite cyclothem (1, for example cyclothem III or IV) and an incomplete cyclothem (2, for example II); compare Text-fig. 5. Not to scale; adapted from Remin *et al.* (2022a).

8; compare Miller and Byrne 1966; Komar and Wang 1984) are at greater risk of entrainment – simply saying, to move forward or transmit, at least occasionally, to the suspension (contrary to rutile).

The settling velocity is another factor influencing hydraulic sorting. As we calculated, based on the formula of Ferguson and Church (2004), the settling velocity is highest for dense rutile grains (Text-fig. 9). This means that the rutile grains settle down first, having additionally a smaller chance to be entrained and even if any, rutile grains, as being denser, will be preferentially rolled along the bottom. The fact that tourmaline grains are larger and lighter, increases the possibility that at least part of the transport will take place in suspension.

Grains that have a lower settling velocity (Text-fig. 9) are preferentially carried further into the sedimentary basin. Due to its much lower density, tourmaline grains are deposited much more slowly than rutile, sustained in the higher portion of the water-flow for a longer period of time (e.g., after flooding), where the flow is strongest (Text-fig. 7). Therefore it is pushed away towards the distal part of the basin enriching the prodelta facies as exemplified in Text-fig. 12 (lover values of RuTidx).

Summarising, the recurring increase in tourmaline abundance (smaller RuTidx; Text-fig. 13), coupled with a simultaneous decrease in rutile abundance in muddy units, most likely resulted from decrease in hydrodynamic power in the depositional environment. This may be interpreted as a transition to a comparatively more distal depositional setting, e.g., further away from the river mouth, thus within the prodelta or an analogous environment (Text-fig. 13).

Analogously, increase in the proportion of rutile (higher RuTidx; Text-fig. 13), and the simultaneous decrease in tourmaline share in the sandy units can be linked to an increase in the flow rate, which might be interpreted as a transition to an environment more proximal to the river discharge, thus representing the delta lobe or similar setting (Text-fig. 13).

Taking all the above physical assumptions concerning the mechanics of grain transport implicates that tourmalines will be preferentially transported to more distal settings in the sedimentary environment whereas rutile will be subjected to relatively shorter transport and will occupy more proximal settings (Text-figs 12 and 13).

The relative increase of RuTidx means more energy. Similarly the lower RuTidx the less energy we have. Therefore, using the RuTidx, we can easily read the relative changes in flow strength/energy of the depositional environment.

CONCLUSIONS

Usage of the RuT index as an effective hydrodynamic power indicator in the sedimentary environment requires that the analysed succession is of sufficient duration, with changes highlighted by e.g., changes in lithofacies, similarly as in the case of the Szozdy Delta System. To emphasise the relative changes in the abundance of these two mineral phases a standardised Z-score statistics must be calculated.

The analysed mineral phases are resistant to diagenetic alteration independently in current surface weathering conditions or during their burial history – even passing through deep burial conditions. The RuTidx, being insensitive to these processes, describes solely the result of hydraulic sorting, thus the hydrodynamic power in the sedimentary environment.

Due to high resistance and ability to thrive multiple recycling, rutile and tourmaline grains are often preserved in the form of very well-rounded grains making them hydraulic sensitive. Therefore, the RuTidx can be used independently of the stratigraphic position of the analysed succession.

The RuTidx may be deduced theoretically, because it fulfils all the physical fundamentals of the transport mechanics of rutile and tourmaline grains. Consequently, the studied case is no more than an empirical confirmation of what can be expected based on physical assumptions that lie behind the RuT index. For that reason, the RuTidx is considered to be valid in any depositional environment where relative changes in hydrodynamic power occur, regardless the age and type of deposit.

Speculating, if this relationship of the abundance of rutile and tourmaline will be confirmed in other sections (which is expected), it might become an easy and effective tool for the recognition of the hydrodynamic power (e.g., flow rate/energy) in the analysed deposits, giving insight into changes of sedimentary environments of any age.

Acknowledgments

Our thanks are extended to Bartosz Gościmski, Joanna Roszkowska-Remin and Martyna Cyglicka for help during fieldwork. Barbara Woronko (University of Warsaw) and an anonymous reviewer are thanked for their constructive comments that markedly improved the final version of the paper. This research was supported by the Polish National Science Centre [Narodowe Centrum Nauki, Polska], under grant number – UMO-2018/29/B/ST10/02947; “Late Cretaceous tectonic evolution of the SE part of the Danish-Polish Trough; revision of the facial architecture and implication for the paleo- and paleobiogeography of Europe”.

REFERENCES:

Ahrens, J.P. 2000. A fall-velocity equation. *Journal of Waterway, Port, Coastal, and Ocean Engineering*, **126**, 99–102.

Błaszkiewicz, A. 1980. Campanian and Maastrichtian ammonites of the Middle Vistula River valley, Poland: a stratigraphic and paleontological study. *Prace Instytutu Geologicznego*, **92**, 1–63.

Cascalho, J. and Fradique, C. 2007. The sources and hydraulic sorting of heavy minerals on the northern Portuguese continental margin. *Developments in Sedimentology*, **58**, 75–107.

Cheng, N.S. 1997. Simplified settling velocity formula for sediment particle. *Journal of Hydraulic Engineering*, **123**, 149–152.

Cyglicki, M. and Remin, Z. submitted. Composition of heavy minerals from the Late Cretaceous Szozdy Delta system, southeastern Polish Basin – implications for source rocks. *Geological Quarterly.*

Dadlez, R., Marek, S. and Pokorski, J. (Eds). 1998. Paleographical Atlas of the Epicontinental Permian and Mesozoic in Poland (1:2 500 000). Polish Geological Institute; Warszawa, Poland. [In Polish]

Dadlez, R., Marek, S. and Pokorski, J. (Eds). 2000. Geological map of Poland without Cenozoic deposits at 1:1 000 000 scale. Polish Geological Institute; Warszawa, Poland. [In Polish]

Dadlez, R., Narkiewicz, M., Stephenson, R.A., Visser, M.T.M. and van Wess, J.D. 1995. Tectonic evolution of the Mid-Polish Trough: modelling implications and significance for central European geology. *Tectonophysics*, **252**, 179–195.

Dietrich, W.E. 1982. Settling velocity of natural particles. *Water Resources Research*, **18**, 1615–1626.

Dubicka, Z. 2015. Benthic foraminiferal biostratigraphy of the lower and middle Campanian of the Polish Lowlands and its application for interregional correlation. *Cretaceous Research*, **56**, 491–503.

Christensen, W.K. 1997b. Palaeobiogeography and migration in the Late Cretaceous belemnite family Belemnitellidae. *Acta Palaeontologica Polonica*, **42**, 457–495.

Ferguson, R.I. and Church, M. 2004. A simple universal equation for grain settling velocity. *Journal of Sedimentary Research*, **74**, 933–937.

Frihy, O.E. 2007. The Nile Delta: processes of heavy mineral sorting and depositional patterns. *Developments in Sedimentology*, **58**, 49–74.

Galehouse, J.S. 1971. Point counting. In: Carver, R.E. (Ed.), Procedures in Sedimentary Petrology, 385–407. Wiley; New York.

Garzanti, E. 2017. The maturity myth in sedimentology and provenance analysis. *Journal of Sedimentary Research*, **87**, 353–365.

Garzanti, E. and Andò, S. 2007. Heavy mineral concentration in modern sands: implications for provenance interpretation. *Developments in Sedimentology*, **58**, 517–545.

Garzanti, E. and Andò, S. 2019. Heavy minerals for Junior Woodchucks. *Minerals*, **9**, 148, 1–25.

Hallermeier, R.J. 1981. Terminal settling velocity of commonly occurring sand grains. *Sedimentology*, **28**, 859–865.

Hammer, Ø. and Harper, D.A.T. 2006. Paleontological Data Analysis, 351 pp. Blackwell Publishing; Malden, Oxford, Carlton.

Hubert, J.F. 1962. A zircon-tourmaline-rutile maturity index and interdependence of the composition of heavy mineral assemblages with the gross composition and textures of sandstones. *Journal of Sedimentary Research*, **32**, 440–450.

Kley, J. and Voigt, T. 2008. Late Cretaceous intraplate thrusting in Central Europe: Effect of Africa-Iberia-Europe convergence, not Alpine collision. *Geology*, **36**, 839–842.

Komar, P.D. 2007. The entrainment, transport and sorting of heavy minerals by waves and currents. *Developments in Sedimentology*, **58**, 3–48.

Komar, P.D. and Wang, C. 1984. Processes of selective grain transport and the formation of placers on beaches. *The Journal of Geology*, **92**, 637–655.

Krzywiec, P. 2006. Structural inversion of the Pomeranian and Kuiavian segments of the Mid-Polish Trough – lateral variations in timing and structural style. *Geological Quarterly*, **50**, 151–168.

Krzywiec, P. 2009. Devonian–Cretaceous repeated subsidence and uplift along the Teisseyre–Tornquist zone in SE Poland – insight from seismic data interpretation. *Tectonophysics*, **475**, 142–159.

Krzywiec, P. and Stachowska, A. 2016. Late Cretaceous inversion of the NW segment of the Mid-Polish Trough – how marginal troughs were formed, and does it matter at all? *Zeitschrift der Deutschen Gesellschaft für Geowissenschaften*, **167**, 107–119.

Krzywiec, P., Stachowska, A. and Stypa, A. 2018. The only way is up – on Mesozoic uplifts and basin inversion events in SE Poland. *Geological Society Special Publications*, **469**, 33–57.

Leszczyński, K. 1997. The Upper Cretaceous carbonate-dominated sequences of the Polish Lowlands. *Geological Quarterly*, **41**, 521–532.

Leszczyński, K. 2010. Lithofacies evolution of the Late Cretaceous basin in the Polish Lowlands. *Biuletyn Państwowego Instytutu Geologicznego*, **443**, 33–54. [In Polish with English summary]

Leszczyński, K. 2012. The internal geometry and lithofacies pattern of the Upper Cretaceous–Danian sequence in the Polish Lowlands. *Geological Quarterly*, **56**, 363–386.

Leszczyński, K. and Dadlez, R. 1999. Subsidence and the problem of incipient inversion in the Mid-Polish Trough based on thickness maps and Cretaceous lithofacies analysis – discussion. *Przegląd Geologiczny*, **47**, 625–628. [In Polish with English summary]

Mange, M.A. and Maurer, H.F.W. 1992. Heavy mineral in color, 147 pp. Chapman and Hall; London.

Miller, R.L. and Byrne, R.J. 1966. The angle of repose of

a single grain on a fixed rough bed. *Sedimentology*, **6**, 303–314.

Morton, A.C. and Hallsworth, C. 1994. Identifying provenance-specific features of detrital heavy mineral assemblages in sandstones. *Sedimentary Geology*, **90**, 241–256.

Morton, A.C. and Hallsworth, C. 1999. Processes controlling the composition of heavy mineral assemblages in sandstones. *Sedimentary Geology*, **124**, 3–29.

Morton, A.C. and Hallsworth, C. 2007. Stability of detrital heavy minerals during burial diagenesis. *Developments in sedimentology*, **58**, 215–245.

Nauton-Fourteu, M., Tyrrell, S. and Morton, A. 2021. Heavy mineral variations in mid-Carboniferous deltaic sandstones: Records of a pre-depositional sediment history? *The Depositional Record*, **7**, 52–63.

Nielsen, S.B. and Hansen, D.L. 2000. Physical explanation of the formation and evolution of inversion zones and marginal troughs. *Geology*, **28**, 875–878.

Odin, G.S. and Lamaurelle, M.A. 2001. The global Campanian-Maastrichtian stage boundary. *Episodes*, **24**, 229–238.

Olszewska, D. 1990. Belemnites from the Upper Cretaceous chalk of Mielnik (eastern Poland). *Acta Geologica Polonica*, **40**, 111–110.

Remin, Z. 2012. The *Belemnella* stratigraphy of the Campanian–Maastrichtian boundary; a new methodological and taxonomic approach. *Acta Geologica Polonica*, **62**, 495–533.

Remin, Z. 2015. The *Belemnitella* stratigraphy of the Upper Campanian – basal Maastrichtian of the Middle Vistula section, central Poland. *Geological Quarterly*, **59**, 783–813.

Remin, Z. 2018. Understanding coleoid migration patterns between eastern and western Europe – belemnite faunas from the upper lower Maastrichtian of Hrebenne, southeast Poland. *Cretaceous Research*, **87**, 368–384.

Remin, Z., Dubicka, Z., Kozłowska, A. and Kuchta, B. 2012. A new method of rock disintegration and foraminiferal extraction with the use of liquid nitrogen [LN2]. Do conventional methods lead to biased paleoecological and paleoenvironmental interpretations? *Marine Micropaleontology*, **86**, 11–14.

Remin, Z., Cyglicki, M., Cybula, M. and Roszkowska-Remin, J. 2015a. Deep versus shallow? Deltaically influenced sedimentation and new transport directions – case study from the Upper Campanian of the Roztocze Hills, SE Poland. In: Proceedings of the 31st IAS Meeting of Sedimentology, Kraków, Poland, p. 438. Polish Geological Society; Kraków.

Remin, Z., Machalski, M. and Jagt, J.W.M. 2015b. The stratigraphically earliest record of *Diplomoceras cylindraceum* (heteromorph ammonite) – implications for Campanian/Maastrichtian boundary definition. *Geological Quarterly*, **59**, 843–848.

Remin, Z., Gruszczyński, M. and Marshall, J.D. 2016. Changes in paleo-circulation and the distribution of ammonite faunas at the Coniacian–Santonian transition in central Poland and western Ukraine. *Acta Geologica Polonica*, **66**, 107–124.

Remin, Z., Cyglicki, M. and Niechwedowicz, M. 2022a. Deep vs. shallow – two contrasting theories? A tectonically activated Late Cretaceous deltaic system in the axial part of the Mid-Polish Trough: a case study from southeast Poland. *Solid Earth*, **13**, 681–703.

Remin, Z., Krzywiec, P. and Stachowska, A. 2022b. Late Cretaceous inversion of SE Polish Basin – syn-depositional tectonics, facies distribution and bathymetric changes. In: Walaszczyk, I. and Todes, J. (Eds), Cretaceous of Poland and of adjacent areas. Field trip Guides, 87–114. Faculty of Geology, University of Warsaw; Poland.

Ryan, P.D., Mange, M.A. and Dewey, J.F. 2007. Statistical analysis of high-resolution heavy minerals stratigraphic data from Ordovician of western Ireland and its tectonic consequences. *Developments in Sedimentology*, **58**, 465–489.

Świdrowska, J. 2007. Cretaceous in Lublin area – sedimentation and tectonic conditions (in Polish with English summary). *Biuletyn Instytutu Geologicznego*, **422**, 63–78.

Voigt, T., Kley, J. and Voigt, S. 2021. Dawn and dusk of Late Cretaceous basin inversion in Central Europe. *Solid Earth*, **12**, 1443–1471.

Walaszczyk, I. 2004. Inoceramids and inoceramid biostratigraphy of the Upper Campanian to basal Maastrichtian of the Middle Vistula River section, central Poland. *Acta Geologica Polonica*, **54**, 95–168.

Walaszczyk, I. and Remin, Z. 2015. Kreda obrzeżenia Gór Świętokrzyskich. In: Skompski, S. (Ed.), LXXXIV Zjazd Polskiego Towarzystwa Geologicznego; Chęciny, 9–11 września, 2015, pp. 41–50. Państwowy Instytut Geologiczny-PIB; Warszawa.

Walaszczyk, I., Dubicka, Z., Olszewska-Nejbert, D. and Remin, Z. 2016. Integrated biostratigraphy of the Santonian through Maastrichtian (Upper Cretaceous) of extra-Carpathian Poland. *Acta Geologica Polonica*, **66**, 313–350.

Yalin, M.S. 1972. Mechanics of sediment transport. 290 pp. Pergamon Press; Oxford, United Kingdom.

Ziegler, P.A. 1990. Geological Atlas of Western and Central Europe, 2nd Edition, 239 pp. Shell Internationale Petroleum Maatschappij and the Geological Society; The Hague and London.

Żelaźniewicz, A., Aleksandrowski, P., Buła, Z., Karnkowski, P., Konon, A., Oszczypko, N., Ślączka, A., Żaba, J. and Żytko, K. 2011. Regionalizacja tektoniczna Polski, 60 pp. Komitet Nauk Geologicznych; Wrocław.

Manuscript submitted: 18th September 2023
Revised version accepted: 6th December 2023

APPENDIX 1

R Code for the prediction of the flow stress τ that is required to threshold or entrainment a grain of certain diameter (based on Komar and Wang 1984); see Text-fig. 8.

```
library(tidyverse)
library(ggplot2)
library(dplyr)
library(scales)

ropQt = 2.650 # density of particle in g/cm3 quartz
ropRu = 4.230 # density of particle in g/cm3 rutile
ropTu = 3.030 # density of particle in g/cm3 tourmaline (dravite end-members)
rof = 1.000 # density of water in kg/m3
g = 980.665 # acceleration due to gravity
K = .025 # average diameter of the bed grains
d = seq(.0088,1, .001)  # diameter of the grains

phi = 61.5*(d/K)**-0.3 # pivoting angle
rad = (phi*2*pi)/360
tg = tan(rad)

tQt = 0.00515*(ropQt-rof)*g*(d**0.568)*tg # threshold stress for quartz grains
tRu = 0.00515*(ropRu-rof)*g*(d**0.568)*tg
tTu = 0.00515*(ropTu-rof)*g*(d**0.568)*tg

df <- data.frame(d, phi, tg, tQt, tRu, tTu)

df <- df %>%
  gather(keys, values, tQt:tTu)
View(df)

ggplot() +
  geom_path(data = df,aes(x = d, y = values, colour = keys), size = 1.3)+
  scale_x_log10(limits = c(0.01, 1), n.breaks = 4,
                labels = trans_format("log10", math_format(10^.x)))+
  scale_y_log10(limits = c(1, 10), n.breaks = 4,
                labels = trans_format("log10", math_format(10^.x)))+
  annotation_logticks()+
  theme_bw()+labs(x = "grain diameter (mm)", y = "threshold stress (dynes/cm2)")
```

APPENDIX 2

R Code for the prediction of the relationship between the settling velocity and the grain diameter for rutile, tourmaline, and quartz (values calculated based on Ferguson and Church 2004); compare Text-fig. 9.

```
library(tidyverse)
library(ggplot2)
library(dplyr)

#Ferguson and Church equation
ropQ = 2650.0 # density of particle in kg/m3 quartz
ropR = 4230.0 # density of particle in kg/m3 rutile
ropT = 3030.0 #density of particle in kg/m3 tourmaline (dravite end-members)
rof = 1000.0 # density of water in kg/m3
visc = 1.002*1E-3 # dynamic viscosity in kPa*s at 20 C
C1 = 18 # constant in Ferguson-Church equation
C2 = 1 # constant in Ferguson-Church equation

Rt = (ropT - rof)/rof
Rr = (ropR - rof)/rof
Rq = (ropQ - rof)/rof

D = seq(0,.001,.000001)
wTourmaline = (Rt*9.81*D**2)/((C1*visc/rof)+((.75*C2*Rt*9.81*D^3)^.5))#tourmaline
settling velocity
wRutile = (Rr*9.81*D**2)/((C1*visc/rof)+((.75*C2*Rr*9.81*D^3)^.5))
wQuartz = (Rq*9.81*D**2)/((C1*visc/rof)+((.75*C2*Rq*9.81*D^3)^.5))
dfFer <- data.frame(D, wTourmaline, wRutile, wQuartz)

DFFER <- dfFer%>%
  gather(keys, SV, wTourmaline:wQuartz) #SV - settling Velocity m/s
View(DFFER)

ggplot(DFFER) +
 aes(x = D*1000, y = SV, colour = keys) + #D*1000 - Diameter of grain in mm
 geom_line(size = .85) +
 geom_vline(xintercept = c(.05,.5))+
 annotate("text", x=.75, y=.15, label= "coarse sand") +
 annotate("text", x=.25, y=.15, label= "fine sand")+
 scale_x_continuous(expand = c(0, 0)) + scale_y_continuous(expand = c(0, 0))+
 theme_bw()+labs(x = "grain diameter (mm)", y = "settling velocity (m/s)")
head(dfFer)
```